11th International Symposium on Turbulence and Shear Flow Phenomena (TSFP11)
Southampton, UK, July 30 to August 2, 2019

GENERATION MECHANISM OF THE HIERARCHY OF VORTICES IN WALL-BOUNDED TURBULENCE

Yutaro Motoori
Graduate School of Engineering Science
Osaka University
1-3 Machikaneyama, Toyonaka, Osaka
y_motoori@fm.me.es.osaka-u.ac.jp

Susumu Goto
Graduate School of Engineering Science
Osaka University
1-3 Machikaneyama, Toyonaka, Osaka
goto@me.es.osaka-u.ac.jp

ABSTRACT

To reveal the generation mechanism of the hierarchy of multiscale vortices in a high-Reynolds-number turbulent boundary layer, we coarse-grain the turbulent velocity field obtained by DNS (Motoori & Goto, 2019*a*,*b*). By using the isosurfaces of the second invariant of the velocity gradient tensor coarse-grained at different scales, we can identify the hierarchy of multiscale vortices in the turbulent boundary layer. Then, we examine the scale-dependent enstrophy production rates contributed from the fluctuation strain-rate fields and from the mean shear to show the following results. (i) In the log layer, vortices smaller than approximately one-fifth of the height are generated by the twice-larger-scale strain-rate fields, whereas larger-scale vortices are generated directly by the mean flow. (ii) In the buffer layer, since all vortices are "large" in the sense that the size is comparable with the height, these vortices are stretched by the mean flow. We also show that the scale at which the qualitative change of the generation mechanism occurs is proportional to the Corrsin scale.

INTRODUCTION

Fully developed turbulence is composed of the hierarchy of multiscale vortices. Although the characteristics of large-scale vortices reflect the information of the boundary condition and/or the external force, small-scale vortices are independent of them. This small-scale universality was predicted by the Kolmogorov similarity hypothesis. Textbooks explain the small-scale universality in terms of the energy cascade, that is, the scale-by-scale energy transfer from large-scale vortices to small-scale vortices. In this process, small-scale statistics become independent of the large-scale properties. The small-scale universality has long been investigated in the wave-number space, however, in the last decades, several studies have focused on the physical mechanism behind it by investigating coherent structures in high-Reynolds-number turbulence. For example, Goto *et al.* (2017) identified the hierarchy of vortices in turbulence in a periodic cube, which is a model of turbulence away from walls, and investigated the interactions among different-scale vortices. We also conducted the direct numerical simulation (DNS) of a high-Reynolds-number turbulent boundary layer and identified the hierarchy of vortices in the *low-pass* filtered field (Motoori & Goto, 2019*a*). Then, the analyses of the low-pass filtered field quantitatively showed the generation mechanism of the hierarchy of multiscale vortices. In the present paper, we further examine the generation mechanism by using the *band-pass* filter because it seems more appropriate for the scale decomposition (Motoori & Goto, 2019*b*). However, we will show that the results are the same as those with the low-pass filter, and they are consistent with the classical picture of the energy cascade.

DIRECT NUMERICAL SIMULATION

We numerically simulate a zero-pressure-gradient turbulent boundary layer by integrating the Navier-Stokes equations for an incompressible fluid, which is the same field reported by Motoori & Goto (2019*a*,*b*). For spatial discretization of the terms in the governing equations, we use a second-order central difference scheme on a staggered grid in the streamwise (x) and spanwise (z) directions, and a non-uniform finite difference scheme in the wall-normal (y) direction. The viscous terms are implicitly integrated by using the second-order Crank-Nicolson method and the convective terms are explicitly integrated by using the second-order Adams-Bashforth method. To generate the inlet condition, we use the time-series data obtained by another DNS (Lee *et al.*, 2013, 2017), which has enabled us to simulate a high-Reynolds-number turbulent boundary layer with relatively small numbers ($6112 \times 616 \times 768$) of grid points. The turbulence in the log layer is fully developed in the sense that the second peak of the premultiplied spanwise energy spectrum of the streamwise velocity component is observed (see figure 2c in Motoori & Goto, 2019*a*). In the present paper, we show the results on the turbulence at the friction-velocity Reynolds number $Re_\tau \approx 1000$ and the momentum-thickness Reynolds number $Re_\theta \approx 3200$.

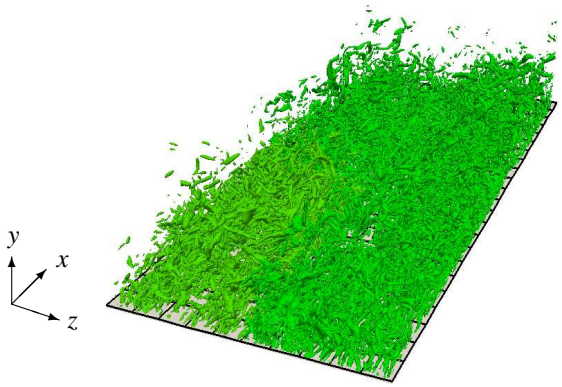

Figure 1. Vortices identified by the isosurfaces of the second invariant Q of the velocity gradient tensor at $Re_\tau \approx 1000$. The threshold is set to be $Q^+ = 4.2 \times 10^{-3}$. The flow is from lower left to upper right. The black grid width is 200 wall units evaluated at the exit plane of the visualized domain.

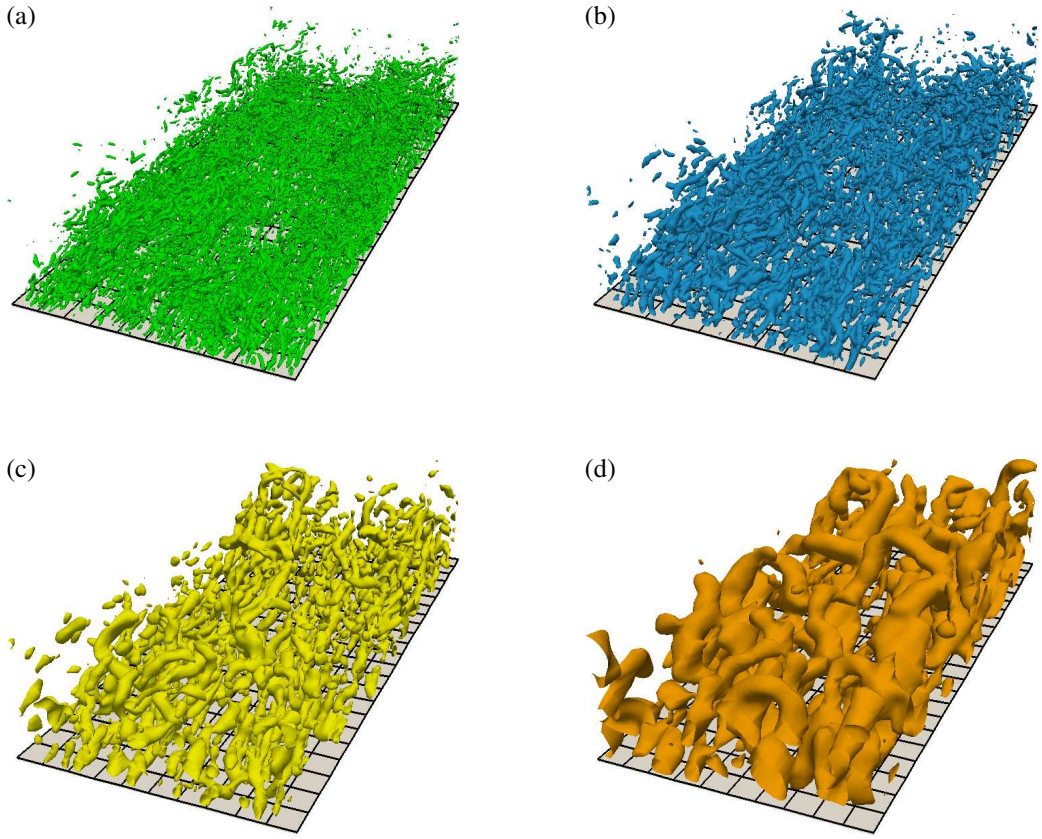

Figure 2. Hierarchy of vortices identified by the isosurfaces of the second invariant $Q^{[\sigma]}$ of the velocity gradient tensor coarse-grained at the scales (a) $\sigma^+ = 20$, (b) 40, (c) 80 and (d) 160, respectively. The thresholds are set to be (a) $Q^{[\sigma]+} = 3.6 \times 10^{-4}$, (b) 1.3×10^{-4}, (c) 3.1×10^{-5} and (d) 2.5×10^{-6}, respectively. The location and instance are the same as in figure 1.

COARSE-GRAINING METHOD

As mentioned in the introduction, vortices with various sizes ranging from large scale (the boundary layer thickness δ_{99}) to small scale (the Kolmogorov scale η) coexist in the turbulent boundary layer. We usually use the velocity gradient when identifying vortical structures. As will be shown in figure 1, however, the structures identified by the velocity gradient reflect only the smallest-scale vortices. Therefore, to understand the interactions and energy exchanges among different-scale vortices, we need to coarse-grain the velocity gradient fields. There are at least two coarse-graining methods (Motoori & Goto, 2019*b*). The first one is a low-pass filter. More specifically, we apply a Gaussian filter to the fluctuation velocity u_i' as

$$u_i^{(\sigma)}(\boldsymbol{x}) = C(y) \int_{V(\boldsymbol{x}|\sigma)} u_i'(\boldsymbol{x}') \exp\left(-\frac{2}{\sigma^2}(\boldsymbol{x}-\boldsymbol{x}')^2\right) \mathrm{d}\boldsymbol{x}', \quad (1)$$

where σ is the filter scale and $C(y)$ is a coefficient to ensure that the summation of the kernel is unity. The velocity $u_i^{(\sigma)}$ coarse-grained at σ includes the information larger than σ. In the sense, this filter corresponds to the low-pass filter of the Fourier modes. The other is a band-pass filter, for which

we take the difference between the low-pass filtered fields at two different scales, i.e.

$$u_i^{[\sigma]}(\boldsymbol{x}) = u_i^{(2\sigma)}(\boldsymbol{x}) - u_i^{(\sigma)}(\boldsymbol{x}). \tag{2}$$

Noting that $u_i^{(\sigma)}$ and $u_i^{(2\sigma)}$, which are obtained by (1), include all scales larger than the filter scale σ and 2σ, respectively, we see that $u_i^{[\sigma]}$ defined by (2) has the contributions from the scales only around σ.

Our previous study (Motoori & Goto, 2019*a*) has investigated the low-pass filtered velocity gradient fields, whereas, in the present paper, we examine the velocity gradient fields coarse-grained by the band-pass filter. As will be shown, there is, however, no difference between the conclusions drawn from the results by using these two filters. Note that all the coarse-grained quantities $.^{[\sigma]}$ are evaluated from the coarse-grained fluctuation velocity $u_i^{[\sigma]}$.

HIERARCHY OF VORTICES

To observe the vortical structures in the turbulent boundary layer, we use the second invariant Q of the velocity gradient tensor. Figure 1 shows isosurfaces of Q where we choose a threshold to visualize vortices in the log layer. In this figure, we only observe the smallest-scale structures. However, multiscale vortices must coexist in turbulence at high Reynolds numbers. In order to identify arbitrary-scale vortices, we apply the band-pass filter to the velocity fields and define the second invariant $Q^{[\sigma]}$ of the coarse-grained velocity gradient tensor. The isosurfaces of a positive value of $Q^{[\sigma]}$ show the regions where the rotation is dominant, that is, vortices with the size σ. We show the isosurfaces of $Q^{[\sigma]}$ coarse-grained at four length scales $\sigma^+ = u_\tau\sigma/\nu = 20$, 40, 80 and 160 in figure 2(a), (b), (c) and (d), respectively. Here, u_τ is the friction velocity and ν is the kinematic viscosity. Note that the grid width drawn on the wall indicates 200 wall units. We can see that the turbulence is composed of the hierarchy of vortices. The scale of the orange objects coarse-grained at $\sigma^+ = 160$ approximately corresponds to the filter scale, and the scale of the green ones at $\sigma^+ = 20$ is about one-eighth as large as that of orange ones. Looking at figure 2(d), we notice that the large-scale ($\sigma^+ = 160$) vortices have spatially organized structures and some of them are arch-like. On the other hand, the small-scale vortices (figure 2a) are similar to the structures (figure 1) without the coarse-graining. Thus, by evaluating the gradients of the coarse-grained velocity fields, we can educe the hierarchy of vortices.

GENERATION MECHANISM

The previous section shows that we are able to identify the hierarchy of vortices. By using the coarse-graining method, we evaluate which scale of the strain rate most significantly contributes to the stretching and amplification of vortices at a given scale. For this purpose, we introduce a quantity,

$$G_S(\sigma_S \to \sigma_\omega; y) = \overline{\left(\frac{\omega_i^{[\sigma_\omega]} S_{ij}^{[\sigma_S]} \omega_j^{[\sigma_\omega]}}{|\boldsymbol{\omega}_i^{[\sigma_\omega]}|^2} \right)\Bigg|_{Q^{[\sigma_\omega]}>0}}, \tag{3}$$

where $\omega_i^{[\sigma_\omega]}$ is the fluctuation vorticity coarse-grained at the scale σ_ω; and $S_{ij}^{[\sigma_S]}$ is the fluctuation rate-of-tensor coarse-grained at the scale σ_S. Since $G_S(\sigma_S \to \sigma_\omega)$ indicates the contribution of the strain rates at σ_S to the enstrophy production rates of the vortices at σ_ω, if G_S is positive (negative), it indicates the stretch (contraction) of the vortices. Here, in order to evaluate the stretching of the vortices identified by the Q criterion, we use the average $\overline{(\cdot)}$ conditioned by $Q^{(\sigma_\omega)} > 0$. In addition, we also define contributions from the mean flow stretching as

$$G_M(\sigma_\omega; y) = \overline{\left(\frac{\omega_i^{[\sigma_\omega]} \overline{S_{ij}} \omega_j^{[\sigma_\omega]}}{|\boldsymbol{\omega}_i^{[\sigma_\omega]}|^2} \right)\Bigg|_{Q^{[\sigma_\omega]}>0}}, \tag{4}$$

where $\overline{S_{ij}}$ is the mean strain rate.

As defined in the previous paragraph, for vortices with the size of a given scale σ_ω at a given height y, G_S indicates the contributions to the enstrophy production rates from the strain rates at σ_S, and G_M indicates those from the mean shear. In this paper, we focus on the dominance of G_S for G_M, and define the ratio as

$$\Gamma(\sigma_S \to \sigma_\omega; y) = \frac{G_S(\sigma_S \to \sigma_\omega; y)}{G_M(\sigma_\omega; y)}. \tag{5}$$

When $\Gamma > 1$, vortices at σ_ω are stretched predominantly by strain rates at σ_S; otherwise, they are stretched mainly by the mean flow.

Let us show in figure 3 the ratio Γ at two different heights (a) $y^+ = u_\tau y/\nu = 200$ and (b) $y^+ = 40$ for $Re_\tau = 1030$. The different symbols indicate the different scales of the stretched vortices. First, looking at the circle symbols ($\sigma_\omega^+ = 20$) in figure 3(a), $\Gamma(2\sigma_\omega \to \sigma_\omega)$ is largest among the contributions from the fluctuating strain rates, and it is larger than 1. This scale $\sigma_\omega^+ = 20$ corresponds to the size of the smallest-scale vortices ($\sigma_\omega/\eta \approx 7$) at the height $y^+ = 200$. Therefore, we can see, in the log layer, that the strain rate twice as large as the stretched vortices contributes most to the stretching rather than the mean flow does. This is also observed in the result for $\sigma_\omega^+ = 40$ (square symbols in figure 3a). In contrast, looking at the triangle symbols ($\sigma_\omega^+ = 80$), since $\Gamma < 1$ for any scales of the strain rates, the contribution of the mean shear is more significant. Therefore, these vortices as large as the height are directly stretched by the mean shear.

Next, looking at the result in the buffer layer (figure 3b), we see that vortices with any scales ($\sigma_\omega^+ = 10$, 20 and 40) are stretched mainly by the mean flow. In this region, there is no scale separation. In other words, all vortices are "large" at the height (but they are, of course, the smallest structures in the whole region). Such large-scale vortices, which are as large as the height, are generated predominantly by the mean flow.

As observed in figure 3, vortices (at $5\eta \lesssim \sigma_\omega \lesssim y$) are stretched predominantly either by the mean shear or by the scale twice as large as themselves. The difference of the generation mechanism depends on the scale of the stretched vortices and the distance from the wall. To quantitatively evaluate the difference, we show in figure 4 the ratio between $G_S(2\sigma_\omega \to \sigma_\omega)$ and $G_M(\sigma_\omega)$, namely $\Gamma(2\sigma_\omega \to \sigma_\omega)$, as a function of σ_ω and y for $Re_\tau = 1030$. Noting that the blue line ($\Gamma = 1$) indicates the scale at which the generation mechanism qualitatively changes, we see that the

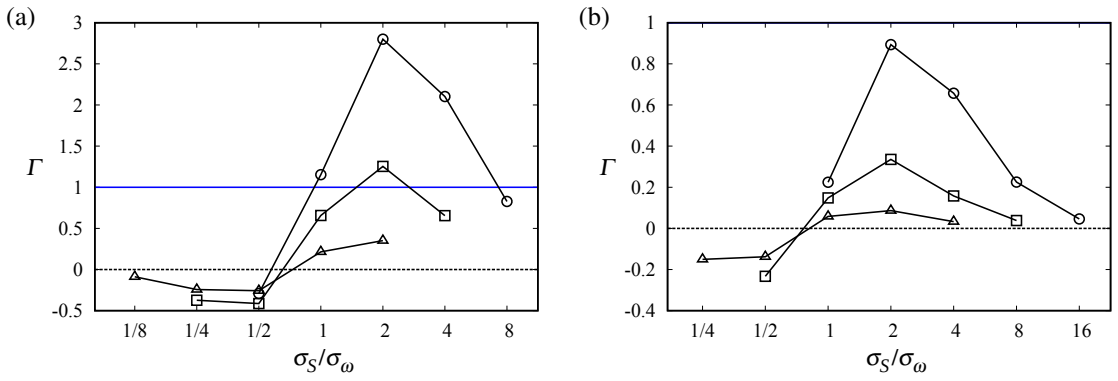

Figure 3. The ratio (5) between the contribution of strain rates coarse-grained at σ_S to the enstrophy production rates of vortices coarse-grained at (a) $\sigma_\omega^+ = 20$ ($\circ$), 40 ($\square$) and 80 ($\triangle$), and (b) 10 ($\circ$), 20 ($\square$) and 40 ($\triangle$) and the contribution of the mean flow at (a) $y^+ = 200$ and (b) 40 at $Re_\tau = 1030$. Blue horizontal line indicates $\Gamma = 1$ (at which the change of the generation mechanism occurs).

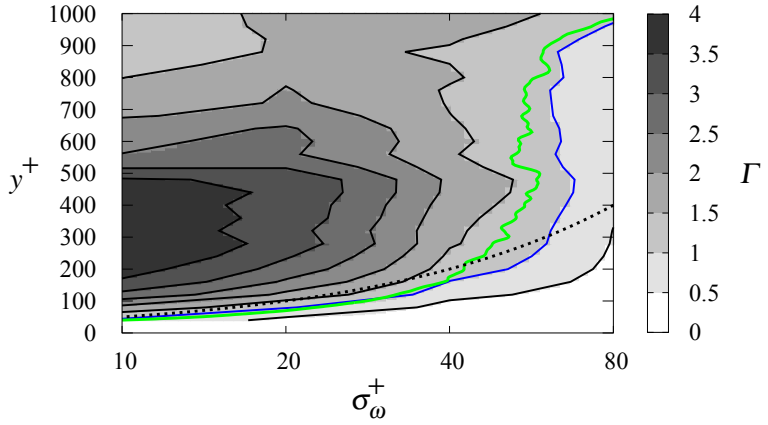

Figure 4. The ratio $\Gamma(2\sigma_\omega \to \sigma_\omega)$ between the contribution of strain rates coarse-grained at $2\sigma_\omega$ to the enstrophy production rates of vortices coarse-grained at σ_ω and the contribution of the mean flow as a function of σ_ω and y at $Re_\tau = 1030$. Blue line; $\Gamma = 1$, green line; $\sigma_\omega = 0.7L_c$; black dotted line, $\sigma_\omega = y/5$.

change occurs at the height $y^+ \approx 5\sigma_\omega^+$ (black dashed line) for $y^+ \lesssim 200$. In other words, in the log layer, whereas the small-scale ($\sigma_\omega \lesssim y/5$) vortices are stretched predominantly by the twice-larger-scale strain rates, the large-scale ($\sigma_\omega \gtrsim y/5$) vortices are mainly stretched by the mean shear. It is also important that the scale (blue line) where $\Gamma = 1$ is in good agreement with the green line, which denotes the Corrsin scale $L_c = \varepsilon^{1/2} S^{-3/2}$ (Corrsin, 1958; Jiménez, 2013). Here, ε is the mean dissipation rate and S is the shear rate of the mean velocity. This is because the mean-shearing time scale S^{-1} is balanced against the cascading time scale $\ell^{2/3}\varepsilon^{-1/3}$ when $\ell \approx L_c$. The observation that the change of the generation mechanism occurs at $\sigma_\omega \approx y/5 \approx 0.7L_c$ is consistent with the fact that $L_c \approx 0.3y$ in the log layer (Jiménez, 2013).

In conclusion, in the log layer with the scale-separation, the generation mechanism of small-scale vortices ($\sigma_\omega \lesssim y/5$) is qualitatively different from the one in the buffer layer. Namely, they are stretched and amplified predominantly by the strain-rates twice as large as themselves.

CONCLUSION

To understand the generation mechanism of multiscale vortical structures, we have conducted DNS of a turbulent boundary layer at high Reynolds numbers. By evaluating the gradient of the coarse-grained velocity, we identify the hierarchy of vortices in the turbulent boundary layer. To investigate the interactions among multiscale vortices and the mean shear, we decompose the velocity field into the mean and fluctuations, and we further decompose the fluctuation fields into different scales by using the band-pass filter (2). We then examine the ratio Γ between two contributions, which are defined by (3) and (4), to the enstrophy production term from scale-dependent fluctuation strain-rate fields and from the mean flow to show the followings. (i) In the log layer, vortices smaller than about the one-fifth of the height are predominately stretched and amplified by strain-rate fields at the scale twice larger than themselves, whereas larger vortices are directly stretched and amplified by the mean shear (figures 3a and 4). (ii) In the buffer layer, all vortices are "large" in the sense that they are as large as the height, and therefore they are stretched and amplified by the mean shear (figures 3b and 4).

We emphasize that these results are obtained by using the band-pass filter (2) and that they are the same as those (see Motoori & Goto, 2019*a*) obtained by the low-pass filter (1). This implies that, since the velocity gradients are predominantly determined by the smallest scale (i.e. the filter scale), the property of the coarse-grained velocity gradients is qualitatively independent of the choice of the coarse-

graining method, although the band-pass filter is more appropriate for detailed analyses (Motoori & Goto, 2019*b*).

By using the same technique developed in our studies, the analyses of turbulent channel flow at high Reynolds numbers are also in progress and will be reported in the conference.

Acknowledgements

We are thankful to Dr. T. A. Zaki and Dr. S. Y. Jung for providing us with their turbulent inlet data. This work was partly supported by JSPS Grant-in-Aid for Scientific Research No.16H04268, and the DNS was conducted under the auspices of the NIFS Collaboration Research Programs (NIFS17KNSS101 and NIFS18KNSS108).

REFERENCES

Corrsin, S. 1958 Local isotropy in turbulent shear flow. *NACA RM* **58B11**.

Goto, S., Saito, Y. & Kawahara, G. 2017 Hierarchy of antiparallel vortex tubes in spatially periodic turbulence at high Reynolds numbers. *Physical Review Fluids* **2**, 064603.

Jiménez, J. 2013 Near-wall turbulence. *Physics of Fluids* **25**, 101302.

Lee, J., Jung, S. Y., Sung, H. J. & Zaki, T. A. 2013 Effect of wall heating on turbulent boundary layers with temperature-dependent viscosity. *Journal of Fluid Mechanics* **726**, 196–225.

Lee, J., Sung, H. J. & Zaki, T. A. 2017 Signature of large-scale motions on turbulent/non-turbulent interface in boundary layers. *Journal of Fluid Mechanics* **819**, 165–187.

Motoori, Y. & Goto, S. 2019*a* Generation mechanism of a hierarchy of vortices in a turbulent boundary layer. *Journal of Fluid Mechanics* **865**, 1085–1109.

Motoori, Y. & Goto, S. 2019*b* Scale-dependent enstrophy production rates in a turbulent boundary layer. Submitted to *Journal of Fluid Science and Technology*.